RESEARCH ARTICLE

NANO · MICRO small
www.small-journal.com

Synergistic Effect of Cation and Anion Passivation Defects and Suppression of Phase Transition Enhance the Performance and Stability of Inverted Perovskite Solar Cells

Yunxin Zhang, Guodong Zhang, Haolin Lu, Hongbin Chen, Yuchuan Shao, Yifan Zheng,* Fulin Sun, Bing Sun, Hao-Li Zhang, Yongsheng Chen, and Guankui Long**

The trap states and phase instability of perovskite films harm the fabrication of high-performance and stable perovskite solar cells (PSCs). Herein, the β-fluorophenylethanammonium cation (β-FPEA$^+$) and tosylate anions (TsO$^-$) are employed to enhance both the performance and stability of inverted PSCs. Theoretical calculations show that β-FPEA$^+$TsO$^-$ can passivate the defects at both FA-I and Pb-I terminals. Nuclear magnetic resonance reveals strong interactions between β-FPEA$^+$TsO$^-$ and perovskites, which facilitate the fabrication of high-quality perovskite films. During crystallization, β-FPEA$^+$ preferentially generates the 2D perovskite, stabilizing the black phase and passivating defects of the perovskite film. Meanwhile, the large TsO$^-$ can be extruded to the grain boundary and surface, reducing trap states and inhibiting the degradation of the perovskite film. The synergistic effect of β-FPEA$^+$ and TsO$^-$ passivation on defects and suppression of phase transition results in the power conversion efficiency (PCE) improved to 25.47% (vs 23.08% of the control), along with the unencapsulated device retaining 81% of initial PCE after 960 h at 85 °C in vacuum. This work provides a novel and simple strategy for designing the combination of large organic cations and non-halogenated anions to passivate the defects and suppress phase transition, thereby achieving high performance and stable PSCs.

1. Introduction

Owing to the excellent photoelectric conversion efficiency, hybrid organic–inorganic perovskite has drawn tremendous attention recently in the field of photovoltaics,[1–6] photodetectors,[7,8] light-emitting diodes[9–12] and spintronic devices.[13,14] Currently, the certified power conversion efficiency (PCE) of perovskite solar cells (PSCs) has exceeded 26%.[15–17] However, the ionic nature of perovskite materials and solution-based fabrication led to numerous trap states, further limiting the development of the device's PCE and stability.[18,19] In particular, the low formation energy between halide and cation vacancy leads to the degradation and performance losses of PSCs.[20] Hence, various strategies have been proposed to eliminate the defects to enhance the PCE and stability of PSCs. Utilizing the combination of larger organic cations and halide anions to form 2D layers is the widely employed strategy to passivate the defects. For example, Yang et al. coated *n*-butylammonium bromide on top of 3D perovskite film and achieved a self-passivated 2D/3D perovskite in the bulk to suppress the non-radiative recombination loss of the perovskite.[21] Li et al. introduced 2-aminoindan hydrochloride into the perovskite precursor inks to construct the 2D/3D heterojunction at the buried interface to minimize the interfacial non-radiative recombination losses toward high-performance inverted MA-free PSCs.[22]

Y. Zhang, H. Lu, F. Sun, G. Long
Tianjin Key Lab for Rare Earth Materials and Applications
Smart Sensing Interdisciplinary Science Center
Renewable Energy Conversion and Storage Center (RECAST)
School of Materials Science and Engineering
Nankai University
Tianjin 300350, China
E-mail: longgk09@nankai.edu.cn

G. Zhang, Y. Shao, Y. Zheng
Key Laboratory of Materials for High-Power Laser
Shanghai Institute of Optics and Fine Mechanics
Chinese Academy of Sciences
Shanghai 201800, China
E-mail: guodongzhang@siom.ac.cn; yifanzheng@siom.ac.cn

The ORCID identification number(s) for the author(s) of this article can be found under https://doi.org/10.1002/smll.202503256

DOI: 10.1002/smll.202503256

B. Sun, H.-L. Zhang
State Key Laboratory of Applied Organic Chemistry (SKLAOC)
Key Laboratory of Special Function Materials and Structure Design (MOE)
College of Chemistry and Chemical Engineering
Lanzhou University
Lanzhou 730000, China

Y. Zhang, H. Chen, Y. Chen
State Key Laboratory and Institute of Elemento-Organic Chemistry
Frontiers Science Center for New Organic Matter
The Centre of Nanoscale Science and Technology and Key Laboratory of Functional Polymer Materials
Renewable Energy Conversion and Storage Center (RECAST)
College of Chemistry
Nankai University
Tianjin 300071, China

Liu et al. employed aromatic formamidinium hydrochloride to develop the 2D/3D hybrid PSCs and obtained an excellent PCE of 23.36%.[23] Yang et al. employed the 4-amidinopyridine hydrochloride to construct the 2D/3D heterostructure based on $FAPbI_3$ perovskites and achieved high PCE values on both rigid and flexible substrates.[24] Our previous work demonstrated that β-fluorophenylethanammonium cation (β-$FPEA^+$) could stabilize the black phase of $FAPbI_3$ and decrease trap states.[25]

Non-halogenated anion also exerts a crucial role in passivating the defects and improving the PCE and stability of PSCs. For example, Jeong et al. employed the format to remove the halide vacancies to eliminate defects in $FAPbI_3$ perovskite films.[26] Wang et al. utilized 1-buty-3-methylimidazolium methanesulfonate as a precursor additive to realize the in situ dual-interface passivation.[27] Yang et al. introduced thiocyanate ammonium into $FAPbI_3$ films to promote the formation of the black phase with better crystallinity.[28] Yang et al. demonstrated that sulfate and phosphate ions can form a wide-bandgap lead oxysalt layer to stabilize the perovskite surface and bulk.[29] Zhang et al. found that trifluoroacetate could passivate the undercoordinated Pb^{2+} and iodide vacancies, thereby suppressing iodide ion migration.[30] Zhuang et al. also utilized the sulfonic acid derivative to passivate the Pb-related defects at the perovskite surface.[31] Wu et al. employed the sulfonic acid group of tridecafluorohexane-1-sulfonic acid potassium to anchor the undercoordinated Pb^{2+} ions to reduce the nonradiative recombination losses at the perovskite interface.[32] Therefore, utilizing the synergistic effect of large organic cations and non-halogenated anions should be an effective strategy for passivating defects and improving the PCE and stability of PSCs.

Herein, the β-$FPEA^+$ functionalized halide and tosylate anions (TsO^-) were designed and employed to simultaneously passivate the defects and stabilize the α-$FAPbI_3$ phase. Density functional theory (DFT) calculations found that β-$FPEA^+TsO^-$ could passivate the defects at both the FA-I and Pb-I terminals. Nuclear magnetic resonance revealed strong interactions between β-$FPEA^+TsO^-$ and perovskite, which should facilitate the fabrication of high-quality perovskite films. During crystallization, β-$FPEA^+$ preferentially forms the 2D perovskite, thus stabilizing the black phase and passivating the defects in the perovskite film. Meanwhile, the larger TsO^- groups were extruded to the grain boundary and surface, which not only reduces the trap states but also suppresses the degradation of the perovskite film. The synergistic effect of β-$FPEA^+$ and TsO^- effectively improved the quality of perovskite film with reduced defects, boosting the efficiency increase from 23.08% to 25.47%, along with the unencapsulated device retaining 81% of initial PCE after 960 h at 85 °C in vacuum. Our work provides a novel and simple strategy to design the combination of large organic cations and non-halogenated anions to passivate the defects and suppress the phase transition, thereby achieving high performance and stable PSCs.

2. Results and Discussion

In previous reports, most attention has been paid to combining larger ammonium cations with halide anions to passivate the trap states. However, the effects of cation and anion are equally important in improving the efficiency and stability of PSCs. Therefore, we combined β-$FPEA^+$ with halide and TsO^- to explore the synergistic effect of cation and anion on the device performance and stability. First, the Vienna ab initio simulation package (VASP) was used to perform the density functional theory (DFT) calculations to investigate the effect of β-$FPEA^+Cl^-$ (Target 1), β-$FPEA^+Br^-$ (Target 2), β-$FPEA^+I^-$ (Target 3) and β-$FPEA^+TsO^-$ (Target 4) (Structures are shown in Figure S1, Supporting Information) on the adsorption and binding onto the defect-free and defected perovskite surface.[33] **Figure 1a** shows the schematic diagrams of FA-I terminated surface defects of FA-vacancy (V_{FA}) and iodine-vacancy (V_I) binding interactions with β-$FPEA^+$ and TsO^-. As presented in Figure 1b, in the FA-I terminated surface model, the V_{FA} formation energy (2.731 eV) is higher than that of V_I (1.101 eV), indicating that V_I is easily formed. The lowest binding energy of −4.629 eV for β-$FPEA^+$ treated V_{FA} in the FA-I terminated surface indicated that the β-$FPEA^+$ tends to insert into the inorganic octahedral lattice in the V_{FA} defect model preferentially generates 2D perovskite, which is advantageous for stabilizing the α-phases of perovskite films.[25] The binding energy of V_I is −4.52, −0.674, −0.964, and −1.101 eV for TsO^-, Cl^-, Br^- and I^- treated the FA-I terminated surface, respectively, suggesting TsO^- is more effective than other halide anions in passivating V_I induced defects, which benefit for limiting the phase transition.[18] The schematic diagrams of the Pb-I terminated surface with the binding interactions with TsO^- with defects of V_{Pb} and V_I' are shown in Figure 1c. The V_{Pb} formation energy (1.911 eV) is higher than V_I' (1.007 eV, Figure 1d), indicating that V_I' is easily formed on the Pb-I terminated surface model, which will cause degradation of the black phase.[18] The binding energy of V_I' and V_{Pb} are −4.201/−1.192, −0.680/0.365, −0.902/−0.057, and −1.007/−0.799 eV for TsO^-, Cl^-, Br^- and I^- treated the Pb-I terminated surface, respectively. Suggesting that TsO^- has a better ability to passivate the defects induced by V_{Pb} and V_I' on the Pb-I terminated surface. Based on the results discussed above, β-$FPEA^+TsO^-$ has good defect passivation ability at both FA-I and Pb-I terminals. The density of states (DOS) was used to determine the impact of Targets 1–4 on the trap states. As shown in Figure 1e, the defect-free surface illustrates no obvious DOS variation at the Fermi level (0 eV). However, the V_{FA} and V_I vacancies appeared, and the DOS intensity increased in the FA-I terminated surface. Then, the surface states near the valence band maximum region are suppressed after treating by β-$FPEA^+$ functionalized with TsO^- and halide anions on the FA-I terminated surface. As shown in Figure 1f,g, the Pb-I terminated surface states are treated by TsO^- and exhibit a defect-free state, demonstrating the ability of TsO^- to suppress defects. These results indicate that the β-$FPEA^+TsO^-$ plays a significant role in reducing the trap states, which positively enhances the efficiency and limits the phase transition of PSCs.[18,20,34]

Based on the calculated results, Target 4 has the potential to fabricate high-quality perovskite films with fewer defects. To evaluate the effect of Targets 1, 2, 3, and 4 on the device performance, the inverted PSCs were fabricated with the structure of ITO/NiO_X/2PACz/perovskite/C_{60}/BCP/Ag (**Figure 2a**). The current density–voltage (*J*–*V*) curves and detailed photovoltaic parameters are shown in Figure 2b and **Table 1**. Compared to the control device, all parameters increased in the Target devices. Interestingly, Target 4 shows a significant improvement in various parameters, achieving a champion PCE of 25.47%, with the V_{OC} 1.19 eV, J_{SC} 25.83 mA cm^{-2},

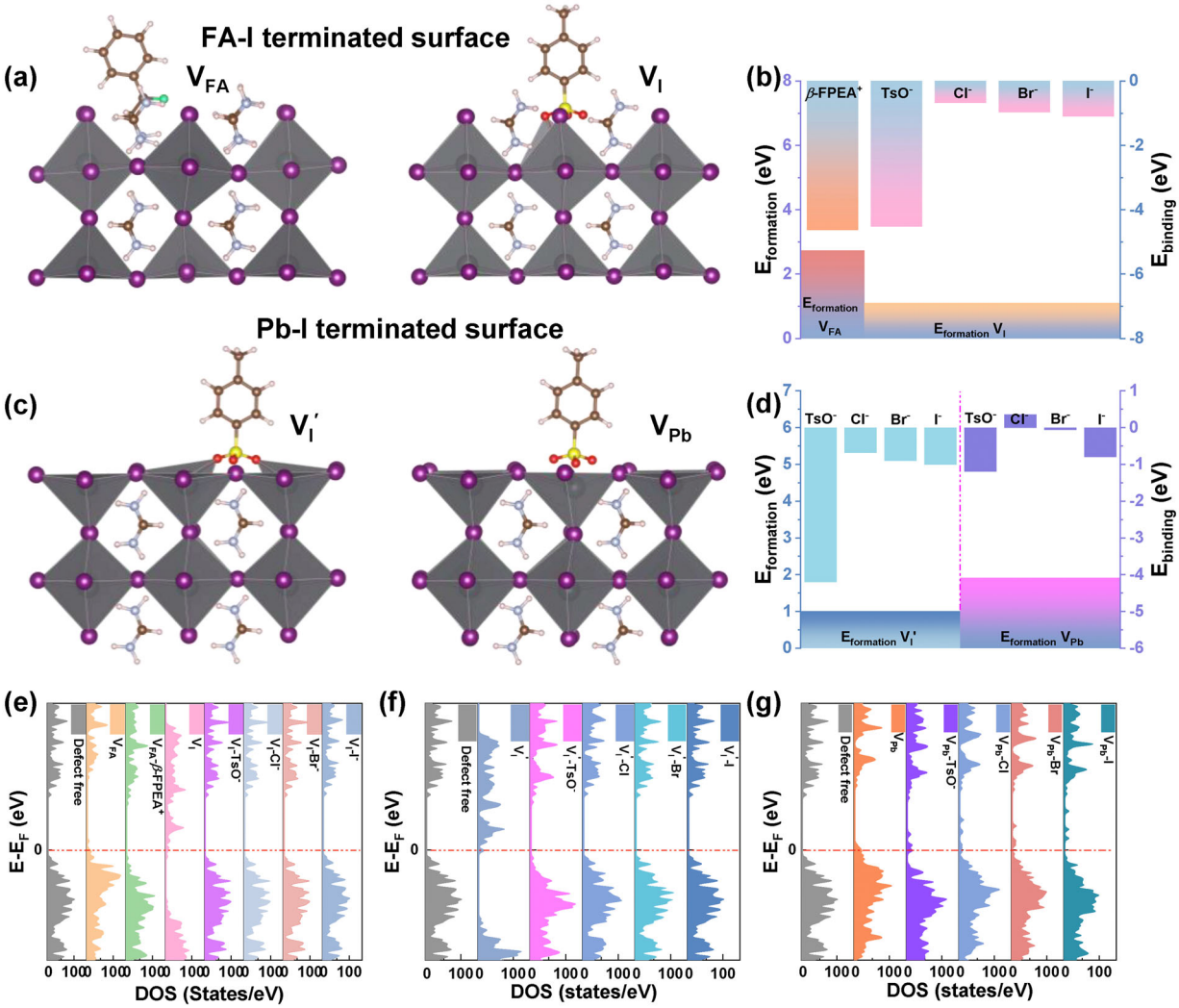

Figure 1. a) Schematic diagrams of binding interactions between β-FPEA$^+$, TsO$^-$, and FA-I terminated surfaces with defects of V_{FA} and V_I. b) The defects formation energy of V_{FA} and V_I defects and binding energy of cation/anions treated the V_{FA} and V_I defects (FA-I terminated surface). c) Schematic diagrams of binding interactions between TsO$^-$ and Pb-I terminated surface with defects of V_I′ and V_{Pb}. d) Defects formation energy of V_{Pb} and V_I′ defects and binding energy of anions treated the V_{Pb} and V_I′ defects (Pb-I terminated surface). e) DOS calculation for perovskite surface structures with defect-free, V_{FA} and V_I upon β-FPEA$^+$ with TsO$^-$, Cl$^-$, Br$^-$ and I$^-$ treatment on FA-I terminated surface. DOS calculation for perovskite surface structures with defect-free, f) V_I′ and g) V_{Pb} upon anions treatment on Pb-I terminated surface.

and FF 83.24%. In contrast, the control device illustrates a moderate PCE of 23.08%, with the V_{OC} 1.17 eV, J_{SC} 24.68 mA cm$^{-2,}$ and FF 79.90%. The PCE distribution of ten devices and optimized β-FPEA$^+$TsO$^-$ doping concentrations are shown in Figure S2 and Table S1 (Supporting Information). Due to the significant improvement in device performance, we focused on Target 4 below. As depicted in Figure 2c, the forward and reverse *J*–*V* curves of Target 4 exhibited negligible hysteresis. The integrated J_{SC} obtained from the external quantum efficiency (EQE) spectra of Target 4 (25.48 mA cm^{-2}, Figure 2d) is consistent with the J_{SC} values obtained from the *J*–*V* curves. The bandgap of the control and Target 4 calculated based on EQE spectra are both 1.55 eV (Figure S3, Supporting Information), which indicates that the addition of the β-FPEA$^+$TsO$^-$ has a negligible effect on the bandgap. The significant improvement in the EQE spectral response of Target 4 is mainly attributed to the addition of the β-FPEA$^+$TsO$^-$ which significantly reduces the trap-induced recombination loss and improves the quality of the Target perovskite film, as discussed below. The steady-state photocurrent and stabilized power output of Target 4 were tested under AM 1.5G illumination as presented in Figure S4 (Supporting Information). Next, the stability of the perovskite film was measured. As shown in Figure 2e,f, the perovskite films were stored for 670 h at room temperature (RT) and 35 ± 5% humidity in air, the control film shows the enhanced X-ray diffraction (XRD) peak intensity of PbI_2 and appeared δ-phases of $FAPbI_3$. Interestingly, the XRD peaks of Target 4 did not change significantly at the same conditions as the control, demonstrating that Target 4 could delay the phase transition and improve environmental stability. The larger water contact angle (81.69° for Target 4 vs 67.37° for control, Figure S5, Supporting Information) of Target 4 could be ascribed to the improved film quality and the hydrophobic groups

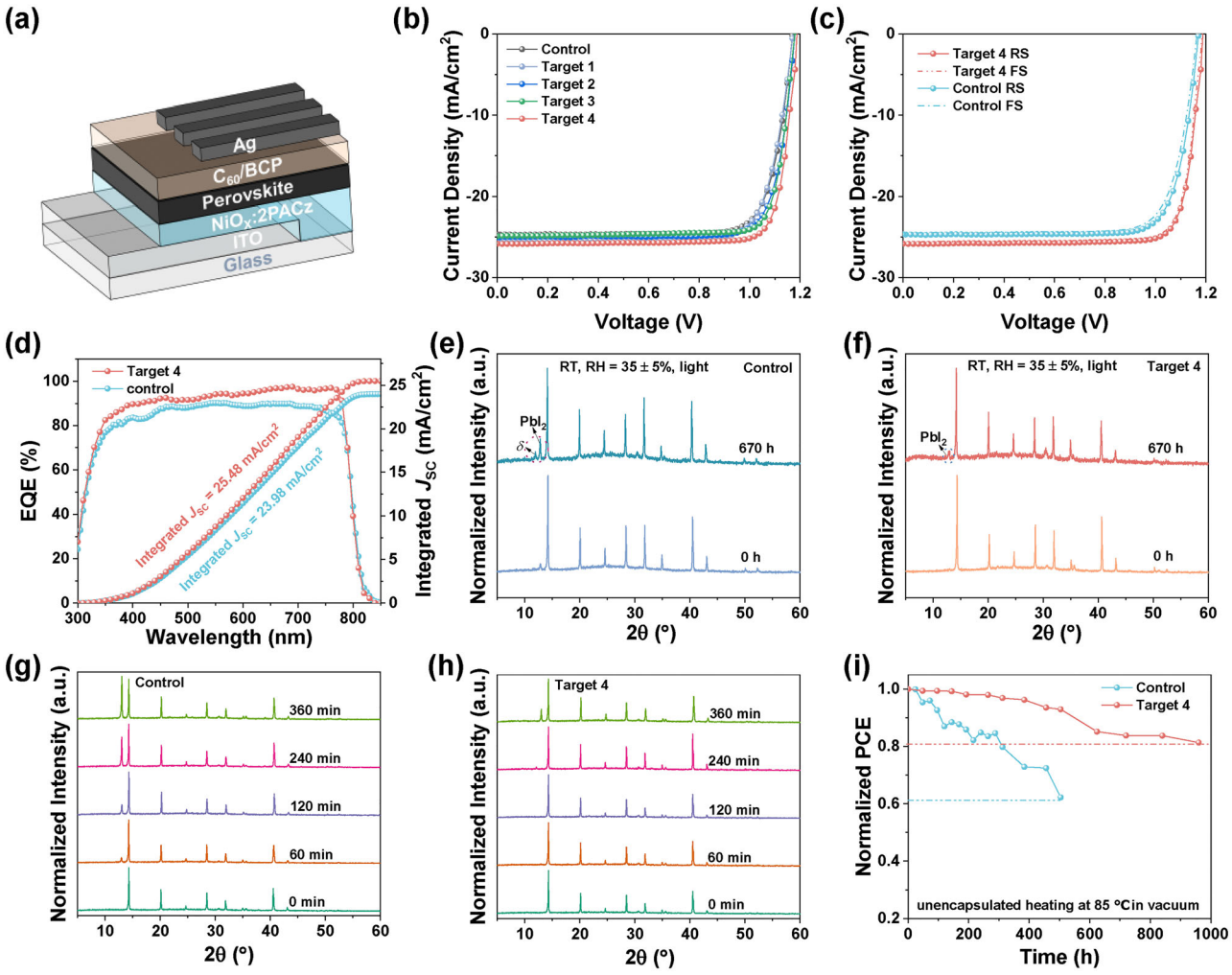

Figure 2. a) Schematic device structure of PSCs. b) *J–V* curves of control, Target 1–4. c) *J–V* curves of Target 4 and control by forward and reverse scan. d) EQE spectra and integrated J_{SC} of Target 4. XRD patterns of e) control and f) Target 4 films stored in RT with RH = 35 ± 5% in air. XRD patterns of g) control and h) Target 4 films heated at 150 °C in the air with a humidity of 35 ± 5%. i) Thermal stability of unencapsulated PSCs heated at 85 °C in vacuum.

of large-sized organic ions in the film (as discussed below), which prevent the moisture invasion and enhance the humidity stability of the perovskite.[35] The thermal stability of the perovskite film is depicted in Figure 2g, the control film was continuously heated for 360 min at 150 °C in air with a humidity of 35 ± 5%, and the intensity of the XRD diffraction peak of PbI_2 gradually increased. Surprisingly, after 360 min of heating under the same conditions as the control, Target 4 appeared a weak XRD diffraction peak of PbI_2 (Figure 2h), which indicated that the Target 4 film has better thermal stability. Then, the unencapsulated device undergoes a long-term thermal stability test at 85 °C in vacuum. As shown in Figure 2i, Target 4 was able to retain 81% of its initial PCE after continuous heating at 85 °C for 960 h. However, under the same condition, the control dropped to 62% after 500 h. It demonstrates that Target 4 has much better thermal stability.

To explore the reasons for performance enhancement, nuclear magnetic resonance (NMR) was used to investigate the chemical interaction between Target 4 and perovskite in solution. As shown in **Figure 3**a, when the β-FPEA$^+$TsO$^-$ were mixed with FAI in DMSO-d_6, the N–H peaks of FAI were shifted from 8.95/8.66 to 9.20/8.92 ppm, and the C–H peak was shifted from 7.86 to 8.07 ppm. The large shift of the C–H peak of FA can be attributed to the strong interaction between FAI and TsO$^-$, which could weaken the FA-I bond to release free I$^-$.[36] By mixing β-FPEA$^+$TsO$^-$ with PbI_2, the N–H peak of β-FPEA$^+$ was shifted from 8.39 to 8.42 ppm (Figure S6, Supporting Information). The C–H peaks of TsO$^-$ also have a significant shift with the mixed

Table 1. The parameters of the optimal devices.

Device	V_{OC} [V]	FF [%]	J_{SC} [mA cm^{-2}]	PCE [%]	PCE_{avg} [%]
Control	1.17	79.90	24.68	23.08	22.7
Target 1	1.17	78.74	25.40	23.44	23.06
Target 2	1.18	80.86	25.03	23.87	23.61
Target 3	1.18	82.73	24.89	24.28	24.14
Target 4	1.19	83.24	25.83	25.47	25.23

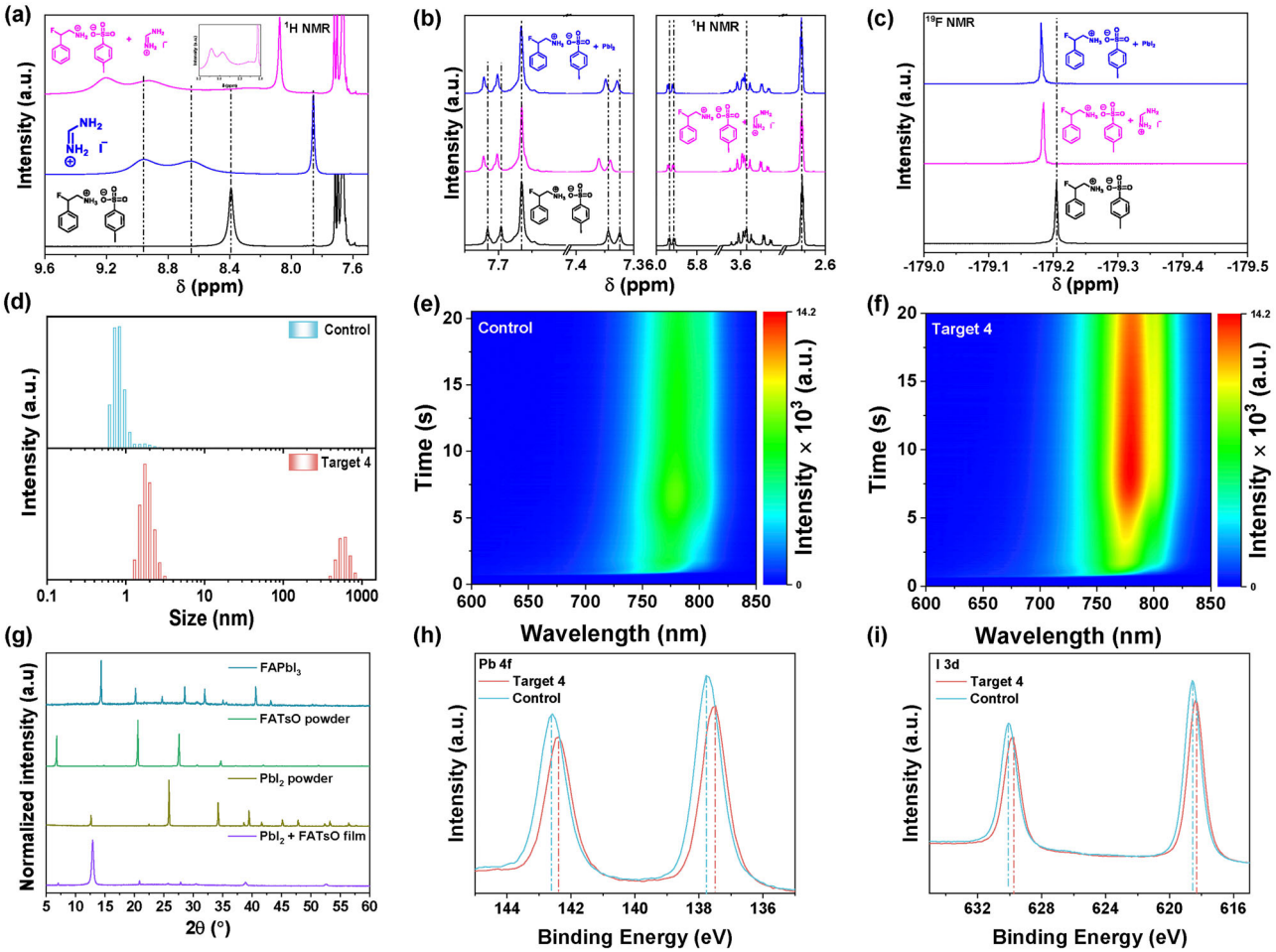

Figure 3. a) ^{1}H NMR spectra of β-FPEA$^+$TsO$^-$, FAI and β-FPEA$^+$TsO$^-$ + FAI, b) ^{1}H NMR and c) ^{19}F NMR spectra of β-FPEA$^+$TsO$^-$, β-FPEA$^+$TsO$^-$ + FAI and β-FPEA$^+$TsO$^-$ + PbI_2. d) DLS spectra of Target 4 and control precursor solutions. In situ PL spectra of e) control and f) Target 4 films. g) XRD patterns of PbI_2 + FATsO (molar ratio 1:1, film), PbI_2 (powder), FATsO (powder), and $FAPbI_3$ (film). XPS spectra of the h) Pb 4f and i) I 3d orbitals of control and Target 4.

solution of β-FPEA$^+$TsO$^-$/FAI and β-FPEA$^+$TsO$^-$/PbI_2 (Figure 3b), demonstrating the stronger interaction between perovskite and TsO$^-$. The F peak of β-FPEA$^+$ also has significant shifts after mixed β-FPEA$^+$TsO$^-$/FAI and β-FPEA$^+$TsO$^-$/PbI_2 (Figure 3c), respectively, which indicates that there is hydrogen bonding interaction between β-FPEA$^+$ and perovskite.[37,38] Then, the dynamic light scattering (DLS) was measured to investigate the effect of Target 4 on the colloidal chemistry of the precursor solutions. As shown in Figure 3d, the precursor solution of Target 4 contained larger clusters and small colloids, which ascribe to the strong interaction between β-FPEA$^+$TsO$^-$ and perovskite.[39] The in situ steady-state photoluminescence (PL) spectra were examined to evaluate the influence of β-FPEA$^+$TsO$^-$ on the formation progress of perovskite film. As presented in Figure 3e,f, Target 4 shows a slower crystallization rate and higher PL intensity than the control, which demonstrates that Target 4 delays crystallization during film formation, increases crystallinity, and improves film quality.[1] As shown in Figure 3g, XRD was used to test whether the TsO$^-$ has been incorporated into the perovskite lattice. When PbI_2 is mixed with FATsO at a molar ratio of 1:1, the XRD only shows the significant peak of PbI_2, indicating that TsO$^-$ cannot be in the perovskite lattice.[30] Compared with the control, the X-ray photoelectron spectroscopy (XPS) peak of Pb 4f and I 3d of Target 4 (Figure 3h,i) has a shift to lower binding energy, which is caused by the interaction between β-FPEA$^+$TsO$^-$ and $[PbI_6]^{4-}$ layer, changing the chemical environment around the Pb and I atoms.[40] As presented in Figure S7 (Supporting Information), the peaks of S 2p could be found, which is attributed to the large anion size that was extruded to the surface and grain boundary during crystallization, which is consistent with the results of time-of-flight secondary ion mass spectrometry (Figure S8, Supporting Information). Additionally, the F 1s signal was identified, and the high-resolution transmission electron microscopy (HR-TEM) image (Figure S9, Supporting Information) illustrates the interplanar lattice spacing of 7.02 Å, which corresponds to the (0120) crystal plane of $(β\text{-FPEA})_2FA_5Pb_6I_{19}$.[25] This phenomenon could be attributed to the preferential formation of the 2D perovskite by β-FPEA$^+$, which serves to stabilize the α-phase of $FAPbI_3$.[25]

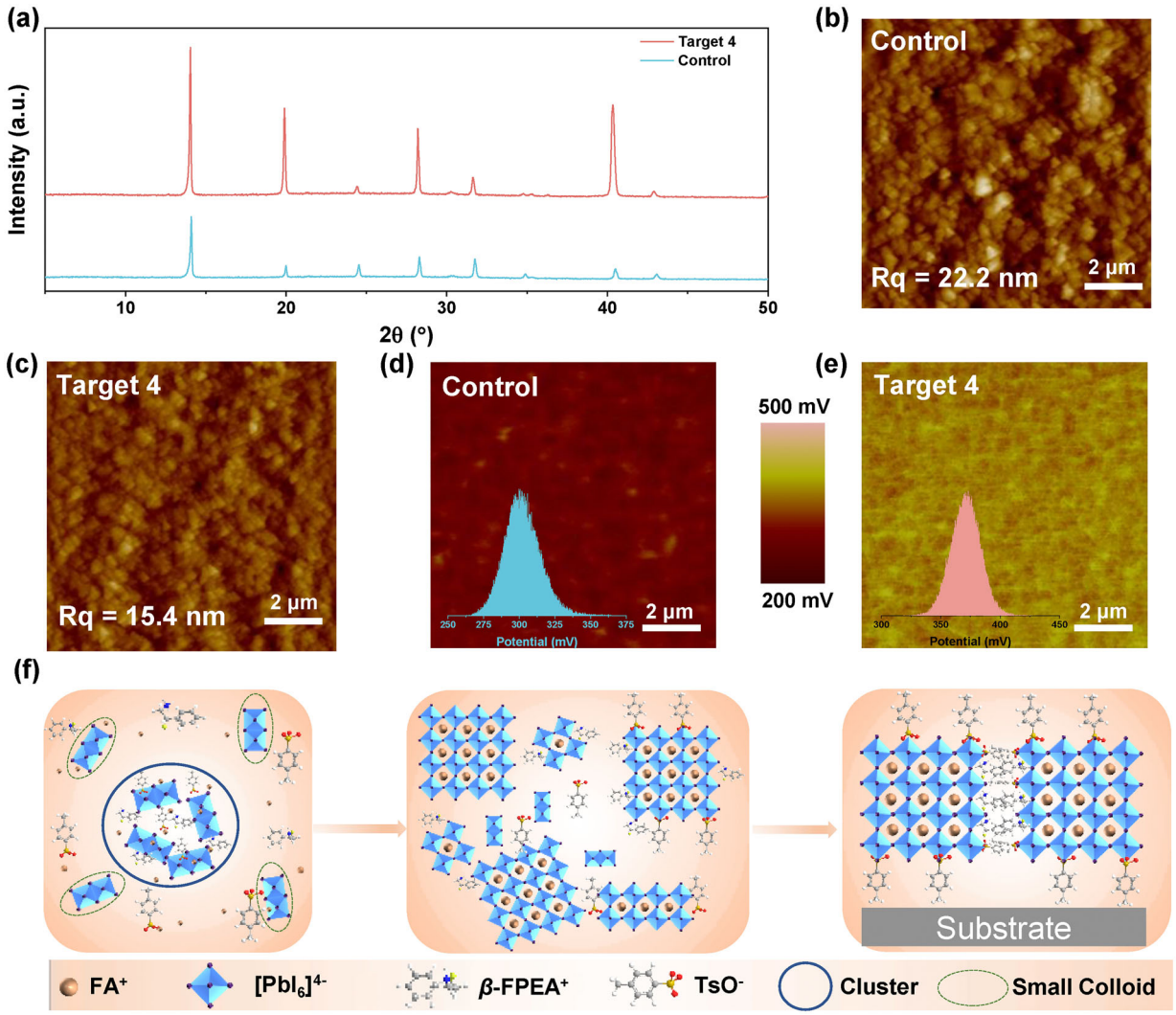

Figure 4. a) XRD patterns of Target 4 and control films. AFM images of b) control and c) Target 4 films. KPFM images of d) control and e) Target 4 films (Insert: statistical distribution of surface potential extracted from the KPFM images). f) Schematic diagram of the film fabrication process.

The crystal quality of the films was determined by XRD and Grazing-incidence wide-angle X-ray scattering (GIWAXS). As shown in **Figures** 4a and S10 (Supporting Information), the Target 4 film displayed higher intensities of (111) and (202) crystal plane diffraction peaks and a larger ratio of (202)/(111) than the control. As displayed in Figure 4b–e and Figure S11 (Supporting Information), Target 4 exhibited a larger grain size, smoother surface with a root-mean-square roughness (R_q) of 15.4 nm (vs control 22.2 nm), and higher surface local potential distributions. These results could be attributed to the superior film crystallinity and regular crystalline arrangement, which is conducive to reducing trap states and enhancing the efficiency of Target 4.[41] Therefore, we inferred the film preparation process from the above data. Due to the stronger interaction between FAI and TsO^-, the FA-I bond was weakened to release free I^- for the formation of $[PbI_6]^{4-}$, thus promoting perovskite crystallization.[36] During the crystallization, the more stable low-dimensional perovskite structures are preferentially formed due to the interaction between β-$FPEA^+$ and $[PbI_6]^{4-}$. The larger size TsO^- are squeezed into the grain boundary and surface, passivating the trap states and improving the film quality.[42]

The UV–vis absorption and PL spectra are shown in **Figure** 5a, the PL intensity of Target 4 is higher than the control, indicating that the high-quality perovskite film formed by Target 4 facilitates charge extraction and reduces charge recombination.[39] As shown in Figure 5b, the longer average lifetime of Target 4 (3.25 μs vs 1.77 μs for control) suggests a significantly reduced trap density and suppressed nonradiative recombination losses, resulting in an enhanced V_{OC}.[43] Thermal admittance spectroscopy results indicate that the defects of Target 4 decrease significantly across the entire energy range (Figure 5c).[27] The much longer photovoltage decay lifetime (30.6 μs vs 5.13 μs) and shorter photocurrent decay lifetime (1.03 μs vs 2.4 μs) of Target 4, as measured by transient photovoltage decay (Figure S12, Supporting Information) and transient photocurrent decay (Figure 5d), indicating the enhanced charge carrier lifetime, improved charge extraction and collection and suppressed nonradiative recombination of Target 4.[44] To further analyze the

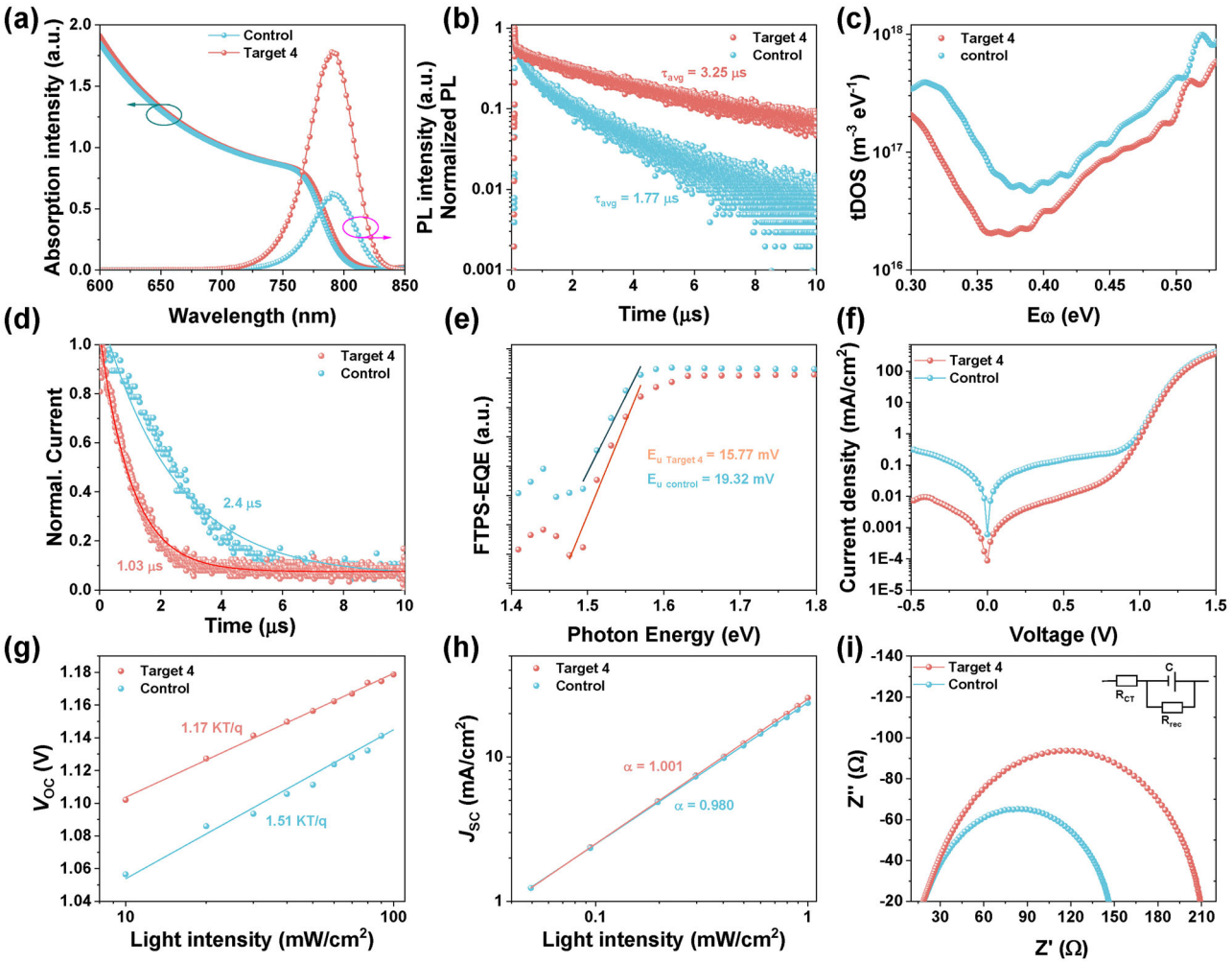

Figure 5. a) UV–vis, PL, and b) TRPL spectra of Target 4 and control film. c) tDOS curves of Target 4 and control. d) TPC decay curves under light conditions. e) FTPS-EQE of Target 4 and control under the optimized condition. f) *J*–*V* curves of Target 4 and control operating in the dark. g) V_{OC} and h) J_{SC} versus light intensity on a seminatural logarithmic scale. i) EIS spectra of Target 4 and control (measured at 1 V bias voltage under dark conditions).

possible reason for the improvement in device performance, the Urbach energy (E_u) was quantified by Fourier transform photocurrent spectroscopy external quantum efficiency (FTPS-EQE). As shown in Figure 5e, sub-bandgap fitting of the FTPS-EQE spectra yields the E_u of 15.77 meV for Target 4 and 19.32 meV for the control devices, respectively. The reduced energy disorder indicates that Target 4 exhibits better crystallinity and lower voltage loss.[45,46] The *J*–*V* curves tested under dark conditions are exhibited in Figure 5f, which confirms that Target 4 has a reduced leakage current.[41,47] The V_{OC} versus the seminatural logarithm of light intensity (Figure 5g) shows a linear relationship with a slope of 1.17 KT q^{-1} for Target 4 (vs control 1.51 KT q^{-1}). The lower slope suggests the suppressed trap-assisted recombination due to the improved film quality and decreased trap states of Target 4. The J_{SC} versus light intensity (Figure 5h) shows a linear correlation on the double logarithmic scale for Target 4 with an α value of 1.001, which is close to 1 and higher than the control of 0.980, indicating less nongeminate recombination due to the reduced grain boundary and trap states, resulting in improved FF and J_{SC} of Target 4.[48,49] In the Nyquist plots (Figure 5i), Target 4 exhibits much lower charge transport resistance (R_{CT}) and higher charge recombination resistance (R_{rec}), suggesting faster charge transport in Target 4 due to the enhanced crystallinity and reduced trap density.[50,51]

3. Conclusion

To reduce the harmful defects of perovskite film in fabricating high-performance and stable PSCs, β-FPEA$^+$TsO$^-$ was designed and employed. DFT results revealed that the incorporation of β-FPEA$^+$ and TsO$^-$ could passivate the defects at both FA-I and Pb-I terminals. The strong interaction between β-FPEA$^+$TsO$^-$ and perovskite could also induce small colloids to aggregate into large clusters and slow the crystallization rate, which is beneficial for fabricating high-quality film. Meanwhile, β-FPEA$^+$ preferentially generates the 2D perovskite, which passivates the defects and stabilizes the black phase. Most importantly, the large TsO$^-$ groups were extruded to the grain boundary and surface during crystallization, which not only reduced the trap states but also improved the stability of the perovskite film. Combined with the

synergistic passivation effect of cations and anions, the PCE was effectively improved from 23.08% to 25.47%, and the unencapsulated device could maintain 81% of its initial efficiency after 960 h of heating under 85 °C in vacuum. Our work provides a novel and simple strategy to utilize the synergistic effect of combining large organic cations and non-halogenated anions to passivate the defects, thus facilitating the achievement of both high-performance and stable PSCs.

Supporting Information

Supporting Information is available from the Wiley Online Library or from the author.

Acknowledgements

The authors gratefully acknowledge the financial support from the NSFC (Grant Number: 92256202, 52473305, 12261131500, 21935007, 52025033) of China, MoST (2022YFB4200400, 2019YFA0705900), the Fundamental Research Funds for the Central Universities, Nankai University (Grant Number: 023–63233038), the NSFC of Tianjin City (20JCZDJC00740), and the 111 Project (B18030). All the theoretical calculations were performed at the Supercomputing Center of Lanzhou University.

Conflict of Interest

The authors declare no conflict of interest.

Data Availability Statement

The data that support the findings of this study are available from the corresponding author upon reasonable request.

Keywords

β-Fluorophenylethanammonium cation, high performance, inverted perovskite solar cells, stability, tosylate anion

Received: March 12, 2025
Revised: April 21, 2025
Published online:

[1] F. Li, X. Deng, Z. Shi, S. Wu, Z. Zeng, D. Wang, Y. Li, F. Qi, Z. Zhang, Z. Yang, S.-H. Jang, F. R. Lin, S. W. Tsang, X.-K. Chen, A. K.-Y. Jen, *Nat. Photonics* **2023**, *17*, 478.
[2] G. Li, Z. Su, L. Canil, D. Hughes, M. H. Aldamasy, J. Dagar, S. Trofimov, L. Wang, W. Zuo, J. J. Jerónimo-Rendon, M. M. Byranvand, C. Wang, R. Zhu, Z. Zhang, F. Yang, G. Nasti, B. Naydenov, W. C. Tsoi, Z. Li, X. Gao, Z. Wang, Y. Jia, E. Unger, M. Saliba, M. Li, A. Abate, *Science* **2023**, *379*, 399.
[3] S. Bai, P. Da, C. Li, Z. Wang, Z. Yuan, F. Fu, M. Kawecki, X. Liu, N. Sakai, J. T. Wang, S. Huettner, S. Buecheler, M. Fahlman, F. Gao, H. J. Snaith, *Nature* **2019**, *571*, 245.
[4] Y. Bai, Z. Huang, X. Zhang, J. Lu, X. Niu, Z. He, C. Zhu, M. Xiao, Q. Song, X. Wei, C. Wang, Z. Cui, J. Dou, Y. Chen, F. Pei, H. Zai, W. Wang, T. Song, P. An, J. Zhang, J. Dong, Y. Li, J. Shi, H. Jin, P. Chen, Y. Sun, Y. Li, H. Chen, Z. Wei, H. Zhou, et al., *Science* **2022**, *378*, 747.
[5] J. C. Blancon, H. Tsai, W. Nie, C. C. Stoumpos, L. Pedesseau, C. Katan, M. Kepenekian, C. M. M. Soe, K. Appavoo, M. Y. Sfeir, S. Tretiak, P. M. Ajayan, M. G. Kanatzidis, J. Even, J. J. Crochet, A. D. Mohite, *Science* **2017**, *355*, 1288.
[6] H. Chen, S. Teale, B. Chen, Y. Hou, L. Grater, T. Zhu, K. Bertens, S. M. Park, H. R. Atapattu, Y. Gao, M. Wei, A. K. Johnston, Q. Zhou, K. Xu, D. Yu, C. Han, T. Cui, E. H. Jung, C. Zhou, W. Zhou, A. H. Proppe, S. Hoogland, F. Laquai, T. Filleter, K. R. Graham, Z. Ning, E. H. Sargent, *Nat. Photonics* **2022**, *16*, 352.
[7] J. Jiang, M. Xiong, K. Fan, C. Bao, D. Xin, Z. Pan, L. Fei, H. Huang, L. Zhou, K. Yao, X. Zheng, L. Shen, F. Gao, *Nat. Photonics* **2022**, *16*, 575.
[8] Y. Jiang, M. Cui, S. Li, C. Sun, Y. Huang, J. Wei, L. Zhang, M. Lv, C. Qin, Y. Liu, M. Yuan, *Nat. Commun.* **2021**, *12*, 336.
[9] Y. Jiang, C. Sun, J. Xu, S. Li, M. Cui, X. Fu, Y. Liu, Y. Liu, H. Wan, K. Wei, T. Zhou, W. Zhang, Y. Yang, J. Yang, C. Qin, S. Gao, J. Pan, Y. Liu, S. Hoogland, E. H. Sargent, J. Chen, M. Yuan, *Nature* **2022**, *612*, 679.
[10] D. Ma, K. Lin, Y. Dong, H. Choubisa, A. H. Proppe, D. Wu, Y.-K. Wang, B. Chen, P. Li, J. Z. Fan, F. Yuan, A. Johnston, Y. Liu, Y. Kang, Z.-H. Lu, Z. Wei, E. H. Sargent, *Nature* **2021**, *599*, 594.
[11] Y.-K. Wang, H. Wan, S. Teale, L. Grater, F. Zhao, Z. Zhang, H.-W. Duan, M. Imran, S.-D. Wang, S. Hoogland, L.-S. Liao, *Nature* **2024**, *629*, 586.
[12] Y. Sun, L. Ge, L. Dai, C. Cho, J. Ferrer Orri, K. Ji, S. J. Zelewski, Y. Liu, A. J. Mirabelli, Y. Zhang, J.-Y. Huang, Y. Wang, K. Gong, M. C. Lai, L. Zhang, D. Yang, J. Lin, E. M. Tennyson, C. Ducati, S. D. Stranks, L.-S. Cui, N. C. Greenham, *Nature* **2023**, *615*, 830.
[13] G. Long, R. Sabatini, M. I. Saidaminov, G. Lakhwani, A. Rasmita, X. Liu, E. H. Sargent, W. Gao, *Nat. Rev. Mater.* **2020**, *5*, 423.
[14] G. Long, C. Jiang, R. Sabatini, Z. Yang, M. Wei, L. N. Quan, Q. Liang, A. Rasmita, M. Askerka, G. Walters, X. Gong, J. Xing, X. Wen, R. Quintero-Bermudez, H. Yuan, G. Xing, X. R. Wang, D. Song, O. Voznyy, M. Zhang, S. Hoogland, W. Gao, Q. Xiong, E. H. Sargent, *Nat. Photonics* **2018**, *12*, 528.
[15] J. Park, J. Kim, H.-S. Yun, M. J. Paik, E. Noh, H. J. Mun, M. G. Kim, T. J. Shin, S. I. I. Seok, *Nature* **2023**, *616*, 724.
[16] Y. Yang, H. Chen, C. Liu, J. Xu, C. Huang, C. D. Malliakas, H. Wan, A. S. R. Bati, Z. Wang, R. P. Reynolds, I. W. Gilley, S. Kitade, T. E. Wiggins, S. Zeiske, S. Suragtkhuu, M. Batmunkh, L. X. Chen, B. Chen, M. G. Kanatzidis, E. H. Sargent, *Science* **2024**, *386*, 898.
[17] H. Chen, C. Liu, J. Xu, A. Maxwell, W. Zhou, Y. Yang, Q. Zhou, A. S. R. Bati, H. Wan, Z. Wang, L. Zeng, J. Wang, P. Serles, Y. Liu, S. Teale, Y. Liu, M. I. Saidaminov, M. Li, N. Rolston, S. Hoogland, T. Filleter, M. G. Kanatzidis, B. Chen, Z. Ning, E. H. Sargent, *Science* **2024**, *384*, 189.
[18] T. Chen, J. Xie, B. Wen, Q. Yin, R. Lin, S. Zhu, P. Gao, *Nat. Commun.* **2023**, *14*, 6125.
[19] F. H. Isikgor, F. Furlan, J. Liu, E. Ugur, M. K. Eswaran, A. S. Subbiah, E. Yengel, M. De Bastiani, G. T. Harrison, S. Zhumagali, C. T. Howells, E. Aydin, M. Wang, N. Gasparini, T. G. Allen, A. u. Rehman, E. Van Kerschaver, D. Baran, I. McCulloch, T. D. Anthopoulos, U. Schwingenschlögl, F. Laquai, S. De Wolf, *Joule* **2021**, *5*, 1566.
[20] N. Li, S. Tao, Y. Chen, X. Niu, C. K. Onwudinanti, C. Hu, Z. Qiu, Z. Xu, G. Zheng, L. Wang, Y. Zhang, L. Li, H. Liu, Y. Lun, J. Hong, X. Wang, Y. Liu, H. Xie, Y. Gao, Y. Bai, S. Yang, G. Brocks, Q. Chen, H. Zhou, *Nat. Energy* **2019**, *4*, 408.
[21] G. Yang, Z. Ren, K. Liu, M. Qin, W. Deng, H. Zhang, H. Wang, J. Liang, F. Ye, Q. Liang, H. Yin, Y. Chen, Y. Zhuang, S. Li, B. Gao, J. Wang, T. Shi, X. Wang, X. Lu, H. Wu, J. Hou, D. Lei, S. K. So, Y. Yang, G. Fang, G. Li, *Nat. Photonics* **2021**, *15*, 681.
[22] H. Li, C. Zhang, C. Gong, D. Zhang, H. Zhang, Q. Zhuang, X. Yu, S. Gong, X. Chen, J. Yang, X. Li, R. Li, J. Li, J. Zhou, H. Yang, Q. Lin, J. Chu, M. Grätzel, J. Chen, Z. Zang, *Nat. Energy* **2023**, *8*, 946.
[23] T. Liu, J. Guo, D. Lu, Z. Xu, Q. Fu, N. Zheng, Z. Xie, X. Wan, X. Zhang, Y. Liu, Y. Chen, *ACS Nano* **2021**, *15*, 7811.

[24] T. Yang, C. Ma, W. Cai, S. Wang, Y. Wu, J. Feng, N. Wu, H. Li, W. Huang, Z. Ding, L. Gao, S. Liu, K. Zhao, *Joule* **2023**, *7*, 574.
[25] Y. Zhang, M. Chen, T. He, H. Chen, Z. Zhang, H. Wang, H. Lu, Q. Ling, Z. Hu, Y. Liu, Y. Chen, G. Long, *Adv. Mater.* **2023**, *35*, 2210836.
[26] J. Jeong, M. Kim, J. Seo, H. Lu, P. Ahlawat, A. Mishra, Y. Yang, M. A. Hope, F. T. Eickemeyer, M. Kim, Y. J. Yoon, I. W. Choi, B. P. Darwich, S. J. Choi, Y. Jo, J. H. Lee, B. Walker, S. M. Zakeeruddin, L. Emsley, U. Rothlisberger, A. Hagfeldt, D. S. Kim, M. Grätzel, J. Y. Kim, *Nature* **2021**, *592*, 381.
[27] H. Wang, Y. Zheng, G. Zhang, P. Wang, X. Sui, H. Yuan, Y. Shi, G. Zhang, G. Ding, Y. Li, T. Li, S. Yang, Y. Shao, *Adv. Mater.* **2023**, *36*, 2307855.
[28] S. Yang, W. Liu, L. Zuo, X. Zhang, T. Ye, J. Chen, C.-Z. Li, G. Wu, H. Chen, *J. Mater. Chem. A* **2016**, *4*, 9430.
[29] S. Yang, S. Chen, E. Mosconi, Y. Fang, X. Xiao, C. Wang, Y. Zhou, Z. Yu, J. Zhao, Y. Gao, F. De Angelis, J. Huang, *Science* **2019**, *365*, 473.
[30] Z. Zhang, M. Li, R. Li, X. Zhuang, C. Wang, X. Shang, D. He, J. Chen, C. Chen, *Adv. Mater.* **2024**, *36*, 2313860.
[31] R. Zhuang, P. Wang, L. Wang, Q. Lai, J. Qiu, Y. Chen, X. Zhang, L. Sun, Y. Hua, *Angew. Chem., Int. Ed.* **2024**, *137*, 202413660.
[32] J. Wu, R. Zhu, G. Li, Z. Zhang, J. Pascual, H. Wu, M. H. Aldamasy, L. Wang, Z. Su, S.-H. Turren-Cruz, R. Roy, F. A. Alharthi, A. Alsalme, J. Zhang, X. Gao, M. Saliba, A. Abate, M. Li, *Adv. Mater.* **2024**, *36*, 2407433.
[33] Y. Zhang, R. Yu, M. Li, Z. He, Y. Dong, Z. Xu, R. Wang, Z. Ma, Z. Tan, *Adv. Mater.* **2023**, *36*, 2310203.
[34] H.-S. Kim, N.-G. Park, *Adv. Energy Mater.* **2024**, *15*, 2400089.
[35] M. Jeong, I. W. Choi, E. M. Go, Y. Cho, M. Kim, B. Lee, S. Jeong, Y. Jo, H. W. Choi, J. Lee, J.-H. Bae, S. K. Kwak, D. S. Kim, C. Yang, *Science* **2020**, *369*, 1615.
[36] X. Guo, W. Zhang, H. Yuan, Z. Cui, W. Li, T. Shu, Y. Li, B. Feng, Y. Hu, X. Li, J. Fang, *Adv. Energy Mater.* **2024**, *15*, 2404293.
[37] X. Fu, T. He, S. Zhang, X. Lei, Y. Jiang, D. Wang, P. Sun, D. Zhao, H.-Y. Hsu, X. Li, M. Wang, M. Yuan, *Chem* **2021**, *7*, 3131.
[38] M. G. Sarwar, B. Dragisic, S. Sagoo, M. S. Taylor, *Angew. Chem., Int. Ed.* **2010**, *49*, 1674.
[39] R. Wang, X. Dong, Q. Ling, Z. Hu, Y. Gao, Y. Chen, Y. Liu, *Angew. Chem., Int. Ed.* **2023**, *62*, 202314690.
[40] T. Zhou, Z. Xu, R. Wang, X. Dong, Q. Fu, Y. Liu, *Adv. Mater.* **2022**, *34*, 2200705.
[41] W. Gao, J. Ding, Q. Ma, H. Zhang, J. Zhang, Z. Zhang, M. Li, Y. Wang, B. Zhang, T. Pauporté, J.-X. Tang, J. Chen, C. Chen, *Adv. Mater.* **2024**, *37*, 2413304.
[42] J. S. Yun, J. Kim, T. Young, R. J. Patterson, D. Kim, J. Seidel, S. Lim, M. A. Green, S. Huang, A. Ho-Baillie, *Adv. Funct. Mater.* **2018**, *28*, 1705363.
[43] J. Guo, B. Wang, D. Lu, T. Wang, T. Liu, R. Wang, X. Dong, T. Zhou, N. Zheng, Q. Fu, Z. Xie, X. Wan, G. Xing, Y. Chen, Y. Liu, *Adv. Mater.* **2023**, *35*, 2212126.
[44] T. Wang, L. Bi, L. Yang, Z. Zeng, X. Ji, Z. Hu, S.-W. Tsang, H.-L. Yip, Q. Fu, A. K. Y. Jen, Y. Liu, *J. Am. Chem. Soc.* **2024**, *146*, 7555.
[45] G. Kim, H. Min, K. S. Lee, D. Y. Lee, S. M. Yoon, S. I. I. Seok, *Science* **2020**, *370*, 108.
[46] S. Cacovich, G. Vidon, M. Degani, M. Legrand, L. Gouda, J.-B. Puel, Y. Vaynzof, J.-F. Guillemoles, D. Ory, G. Grancini, *Nat. Commun.* **2022**, *13*, 2868.
[47] Y. Zhang, S. Chen, H. Chen, G. Zhang, M. Zhao, C. Zhao, W. Guo, W. Ji, Z. Shi, T. Jiu, *J. Mater. Chem. C* **2020**, *8*, 5894.
[48] L. Bai, Z. Yu, L. Liu, Y. Chang, Z. Ma, T. Jiu, *Nano Energy* **2024**, *131*, 110310.
[49] T. Chen, Y. Zhong, T. Duan, X. Tang, W. Zhao, J. Wang, G. Lu, G. Long, J. Zhang, K. Han, X. Wan, B. Kan, Y. Chen, *Angew. Chem., Int. Ed.* **2024**, *137*, 202412983.
[50] Y. Zhang, N.-G. Park, *ACS Energy Lett.* **2022**, *7*, 757.
[51] N. Li, Z. Zhu, C.-C. Chueh, H. Liu, B. Peng, A. Petrone, X. Li, L. Wang, A. K. Y. Jen, *Adv. Energy Mater.* **2017**, *7*, 1601307.